Table 1.6.5.1
$R_{\rm merge}$ values for Ex2 for the 589 sets of general reflections of *mmm* which have all eight measurements in the set

$R_{\rm merge}$ (%)	*mmm*	2*mm*	*m*2*m*	*mm*2	222
R_A	1.30	1.30	1.30	1.30	1.30
R_D	100.0	254.4	235.7	258.1	82.9

Table 1.6.5.2
$R_{\rm merge}$ values for Ex1 for the 724 sets of general reflections of 2/*m* which have all four measurements in the set

$R_{\rm merge}$ (%)	2/*m*	*m*	2
R_A	1.29	1.29	1.29
R_D	100.0	98.3	101.7

data set is unsatisfactorily dominated by random uncertainty and systematic error.

Example 3

The crystals of compound Ex3 (Zhu & Jiang, 2007) occur in Laue group $\overline{1}$. One finds $\text{Friedif}_{\rm stat}$ = 70 and $\text{Friedif}_{\rm obs}$ = 499. The huge discrepency between the two shows that the observed values of D are dominated by random uncertainty and systematic error.

1.6.5.1.3. Resolution of noncentrosymmetric ambiguities

It was shown in Section 1.6.5.1.2 that under certain circumstances it is possible to determine whether or not the space group of the crystal investigated is centrosymmetric. Suppose that the space group was found to be noncentrosymmetric. In each Laue class, there is one centrosymmetric point group and one or more noncentrosymmetric point groups. For example, in the Laue class *mmm* we need to distinguish between the point groups 222, 2*mm*, *m*2*m* and *mm*2, and of course between the space groups based on them. We shall show that it is possible in practice to distinguish between these noncentrosymmetric point groups using intensity differences between Friedel opposites caused by resonant scattering.

An excellent intensity data set from a crystal (Ex2 above) of potassium hydrogen (2*R*, 3*R*) tartrate, measured with a wavelength of 0.7469 Å at 100 K, was used. The Laue group was assumed to be *mmm*. The raw data set was initially merged and averaged in point group 1 and all special reflections of the Laue group *mmm* (*i.e.* 0*kl*, *h*0*l*, *hk*0, *h*00, 0*k*0, 00*l*) were set aside. The remaining data were organized into sets of reflections symmetry-equivalent under the Laue group *mmm*, and only those sets (589 in all) containing all 8 of the *mmm*-symmetry-equivalent reflections were retained. Each of these sets provides 4 $A_{\rm obs}$ and 4 $D_{\rm obs}$ values which can be used to calculate $R_{\rm merge}$ values appropriate to the five point groups in the Laue class *mmm*. The results are given in Table 1.6.5.1. The value of 100% for $R_{\rm merge}$ in a centrosymmetric point group, such as *mmm* or 2/*m*, arises by definition and not by coincidence. The R_D of the true point group has the lowest value, which is noticeably different from the other choices of point group.

The crystal of Ex1 above (space group $P2_1/c$) was treated in a similar manner. Table 1.6.5.2 shows that R_D values display no preference between the three point groups in Laue class 2/*m*.

Intensity measurements comprising a full sphere of reflections are essential to the success of the $R_{\rm merge}$ tests described in this section.

1.6.5.1.4. Data evaluation after structure refinement

There is an excellent way in which to evaluate both data measurement and treatment procedures, and the fit of the model to the data, including the space-group assignment, at the completion of structure refinement. This technique is applicable both to noncentrosymmetric and to centrosymmetric crystals. A scattergram of $D_{\rm obs}$ against $D_{\rm model}$, and $2A_{\rm obs}$ against $2A_{\rm model}$ pairs are plotted on the same graph. All ($D_{\rm obs}$, $D_{\rm model}$) pairs are plotted together with those ($2A_{\rm obs}$, $2A_{\rm model}$) pairs which have $2A_{\rm obs} < |D_{\rm obs}|_{\rm max}$. The range of values on the axes of the model and of the observed values should be identical. For acentric reflections, for both A and D, a good fit of the observed to the model quantities shows itself as a straight line of slope 1 passing through the origin, with some scatter about this ideal straight line. For an individual reflection, $2A$ and D are, respectively, the sum and the difference of the same quantities and they have identical standard uncertainties. It is thus natural to select $2A$ and D to plot on the same graph. In practice one sees that the spread of the $2A$ plot increases with increasing value of $2A$. Fig. 1.6.5.1 shows the $2AD$ plot for Ex2 of Example 2 in Section 1.6.5.1.2, which is most satisfactory and confirms the choice of point group from the use of $R_{\rm merge}$. The conventional R value for all reflections is 3.1% and for those shown in Fig. 1.6.5.1 it is 10.4%. The R value for all D values is good at 51.1%. Fig. 1.6.5.2 shows the $2AD$ plot for Ex1 of Example 1 in Section 1.6.5.1.2. The structure model is centrosymmetric so all $D_{\rm model}$ values are zero. The conventional R value on A for all reflections is 4.3% and for those shown in Fig. 1.6.5.2 it is 9.1%. The R value on all the D values is 100%.

1.6.5.2. Space-group determination in macromolecular crystallography

For macromolecular crystallography, succinct descriptions of space-group determination have been given by Kabsch (2010*a*,*b*, 2012) and Evans (2006, 2011). Two characteristics of macromolecular crystals give rise to variations on the small-molecule procedures described above.

The first characteristic is the large size of the unit cell of macromolecular crystals and the variation of the cell dimensions from one crystal to another. This makes the determination of the Bravais lattice by cell reduction problematic, as small changes of cell dimensions give rise to differences in the assignment. Kabsch (2010*a*,*b*, 2012) uses a 'quality index' from each of Niggli's 44 lattice characters to come to a best choice. Grosse-Kunstleve *et al.* (2004) and Sauter *et al.* (2004) have found that some commonly used methods to determine the Bravais lattice are susceptible to numerical instability, making it possible for high-symmetry Bravais lattice types to be improperly identified. Sauter *et al.* (2004, 2006) find from practical experience that a deviation δ as high as 1.4° from perfect alignment of direct and reciprocal lattice rows must be allowed to construct the highest-symmetry Bravais type consistent with the data. Evans (2006) uses a value of 3.0°. The large unit-cell size also gives rise to a large number of reflections in the asymmetric region of reciprocal space, and taken with the tendency of macromolecular crystals to decompose in the X-ray beam, full-sphere data sets are uncommon. This means that confirmation of the Laue class by means of values of $R_{\rm int}$ ($R_{\rm merge}$) are rarer than with small-molecule crystallography, although Kabsch (2010*b*) does use a 'redundancy-independent R factor'. Evans (2006, 2011) describes methods very similar to those given as the second stage in Section 1.6.2.1. The conclusion of Sauter *et al.* (2006) and Evans (2006) is that $R_{\rm int}$ values as high

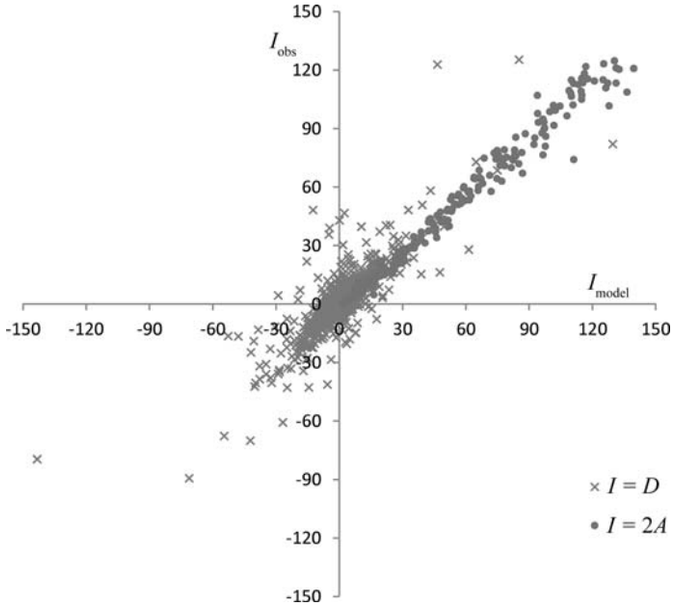

Figure 1.6.5.1
Data-evaluation plot for crystal Ex2. The plot shows a scattergram of all (D_{obs}, D_{model}) pairs and those ($2A_{obs}$, $2A_{model}$) pairs in the same intensity range as the D values.

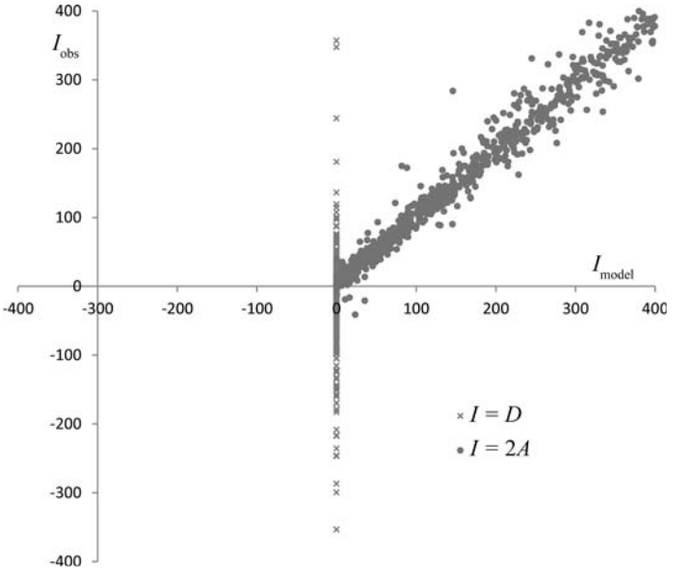

Figure 1.6.5.2
Data-evaluation plot for crystal Ex1. The plot shows a scattergram of all (D_{obs}, D_{model}) and some ($2A_{obs}$, $2A_{model}$) data points.

as 25% must be permitted in order to assemble an optimal set of operations to describe the diffraction symmetry. Another interesting procedure, accompanied by experimental proof, has been devised by Sauter *et al.* (2006). They show that it is clearer to calculate R_{merge} values individually for each potential symmetry operation of a target point group rather than comparing R_{merge} values for target point groups globally. According to Sauter *et al.* (2006) the reason for this improvement lies in the lack of intensity data relating some target symmetry operations.

The second characteristic of macromolecular crystals is that the compound is known, or presumed, to be chiral and enantiomerically pure, so that the crystal structure is chiral. This limits the choice of space group to the 65 Sohncke space groups containing only translations, pure rotations or screw rotations. For ease of use, these have been typeset in bold in Tables 1.6.4.2–1.6.4.30.

For the evaluation of protein structures, Poon *et al.* (2010) apply similar techniques to those described in Section 1.6.2.3. The major tactical objective is to identify pairs of α-helices that have been declared to be symmetry-independent in the structure solution but which may well be related by a rotational symmetry of the crystal structure. Poon *et al.* (2010) have been careful to test their methodology against generated structural data before proceeding to tests on real data. Their results indicate that some 2% of X-ray structures in the Protein Data Bank potentially fit in a higher-symmetry space group. Zwart *et al.* (2008) have studied the problems of under-assigned translational symmetry operations, suspected incorrect symmetry and twinned data with ambiguous space-group choices, and give illustrations of the uses of group–subgroup relations.

1.6.5.3. Space-group determination from powder diffraction

In powder diffraction, the reciprocal lattice is projected onto a single dimension. This projection gives rise to the major difficulty in interpreting powder-diffraction patterns. Reflections overlap each other either exactly, owing to the symmetry of the lattice metric, or approximately. This makes the extraction of the integrated intensities of individual Bragg reflections liable to error. Experimentally, the use of synchrotron radiation with its exceedingly fine and highly monochromatic beam has enabled considerable progress to be made over recent years. Other obstacles to the interpretation of powder-diffraction patterns, which occur at all stages of the analysis, are background interpretation, preferred orientation, pseudo-translational symmetry and impurity phases. These are general powder-diffraction problems and will not be treated at all in the current chapter. The reader should consult David *et al.* (2002) and David & Shankland (2008) or the forthcoming new volume of *International Tables for Crystallography* (Volume H, *Powder Diffraction*) for further information.

It goes without saying that the main use of the powder method is in structural studies of compounds for which single crystals cannot be grown.

Let us start by running through the three stages of extraction of symmetry information from the diffraction pattern described in Section 1.6.2.1 to see how they apply to powder diffraction.

(1) Stage 1 concerns the determination of the Bravais lattice from the experimentally determined cell dimensions. As such, this process is identical to that described in Section 1.6.2.1. The obstacle, arising from peak overlap, is the initial indexing of the powder pattern and the determination of a unit cell, see David *et al.* (2002) and David & Shankland (2008).

(2) Stage 2 concerns the determination of the point-group symmetry of the intensities of the Bragg reflections. As a preparation to stages 2 and 3, the integrated Bragg intensities have to be extracted from the powder-diffraction pattern by one of the commonly used profile analysis techniques [see David *et al.* (2002) and David & Shankland (2008)]. The intensities of severely overlapped reflections are subject to error. Moreover, the exact overlap of reflections owing to the symmetry of the lattice metric makes it impossible to distinguish between high- and low-symmetry Laue groups in the same family *e.g.* between 4/*m* and 4/*mmm* in the tetragonal family and $m\bar{3}$ and $m\bar{3}m$ in the cubic family. Likewise,